Estimating outdoor advertising media visibility with voxel-based approach

Article *in* Applied Geography · October 2017

DOI: 10.1016/j.apgeog.2017.07.007

CITATIONS
31

READS
4,672

2 authors:

Szymon Chmielewski
University of Life Sciences in Lublin
40 PUBLICATIONS **441** CITATIONS

SEE PROFILE

Piotr Tompalski
Natural Resources Canada
100 PUBLICATIONS **3,928** CITATIONS

SEE PROFILE

Estimating outdoor advertising media visibility with voxel-based approach

Chmielewski Szymon [1)], Tompalski Piotr [2)]

[1)] University of Life Sciences in Lublin, Institute of Soil Sciences, and Environmental Engineering and Management, Leszczyńskiego 7 St, 20-069, Lublin, Poland (gisszymon@gmail.com)

[2)] University of British Columbia, Faculty of Forestry, 2424 Main Mall, Vancouver, BC V6T 1Z4, Canada (piotr.tompalski@ubc.ca)

Chmielewski Sz., Tompalski P. (2017). Estimating outdoor advertising media visibility with voxel-based approach. *Applied Geography*, 87: 1-13 (published online 27 July 2017)

To link to this article: **http://dx.doi.org/10.1016/j.apgeog.2017.07.007**

Abstract

Visibility estimation is one of the most fundamental spatial analyses, usually conducted with the use of 2D and 3D GIS tools. The 3D approach requires 3D features that represent the complex character of visibility obstacles. While a bare ground surface can be precisely represented with raster data, and building footprints can be extruded into 3D objects, visibility obstacles created by high vegetation are still challenging to represent in 3D. To analyse visibility in cityscapes with complex vegetation we propose a hybrid model consisting of voxels and raster surfaces. The aim of this study is to assess optimal parameters for airborne laser scanning (ALS) data voxelization for the purpose of visibility analysis. In doing so we are answering two essential questions: 1) what is the optimal ALS point cloud post-spacing distance for accurate 3D visibility modeling using voxels? and 2) what is the right voxel volume for this kind of analysis? We tested several ALS data thinning algorithms and various voxel sizes. Based on 48 visibility tests we propose an optimal model (both accurate and reasonably fast) for 3D visibility modeling. We also propose a novel approach to display visibility results that move on from traditional binary cartographic presentations to the probability of visibility. Our study is focused on a relatively small cityscape object where detailed, large-scale visibility analysis is required. We present our visibility results on the example of a standard (6 x 3 m) advertisement billboard where, visibility, the main impact factor of this medium can be virtually mapped.

1. Introduction

Visibility modelling, one of the most common GIS analyses (O'Sullivan & Turner, 2001), is used to ascertain what an observer may see from a particular vantage point. Visibility approaches are used in multiple fields, including visual impact assessment (Wrożyński, Sojka & Pyszny, 2016); urban design and planning (Fisher-Gewirtzmann, & Wagner, 2003); landscape perception (Sahraoui, Youssoufi and Christophe-Foltete, 2016; Weitkamp, Bregt, van Lammeren, & den Berg 2007; Felleman, 1986) and classification (Brabyn & Mark, 2011; Brabyn, 2015); recreational trail location (Snyder, Whitmore, Schneider & Becker 2008); geomorphology (Mitasova et al. 2012); archaeology (Marsh & Schreiber 2015); and for military applications (Caldwell, 2004). These often long-range visibility analyses are well described in the international literature and usually meet the accuracy requirements necessary for a given application (Bilsen & Stolk, 2008). Visibility analysis can be conducted in either two or three dimensions with the use of raster (e.g. 2D viewshed visibility) or vector-based surface models (e.g. 2D isovist). Three dimensional environment is typically represented with the use of volumetric features, such as voxels, that characterise the complex character of visibility obstacles.

Voxels have been used in a number of different GIS analyses, but only a few of them are concerned visibility phenomenon. For example, Hagstorm, Messinger & Salvaggio (2014) performed tests of various voxelization methods (the fraction of unsampled voxels) on 3D visibility results. Accuracy assessment has also been limited, with some basic visibility layer accuracy assessment presented by Kloucek, Lagner & Símova (2015) for a 2D approach. Results provided by our study give the first overview of the influence of various voxelization methods on ground-truth visibility models. Here we propose a voxel-based method for outdoor advertisement (OA) visibility modelling. OA are one of the most effective means of out-of-home (OOH) media, and this efficacy, besides message content and design, is due to OA visibility. OOH media operates in a complex urban environment, and therefore a detailed short range visibility obstruction model is required for accurate visible area delineation. This can be done with the use of Airborne Laser Scanning (ALS)

technology that enables the collection of 3D point clouds to model visibility obstructions, but to date, no practical applications of ALS voxelized data to OA visibility modelling have been described. Existing attempts to use voxels in visibility modelling (Pyysalo, Oksanen & Sarjakoski 2009; Hagstrom & Messinger 2011; Fisher-Gewirtzman, Shashkov and Doytsher, 2013) do not analyse the influence of ALS data thinning and voxel resolution on visibility modelling accuracy refereed to ground truth model. To achieve this, we propose a three step methodology: First, point clouds are filtered and converted into voxel space using sixteen thinning approaches and three voxel sizes. Second, we test 48 combinations of voxel sizes and filtering methods to find the most accurate OA visibility model. Finally, we map OA visibility in a non-binary way, probabilistically visualizing the level of OA visibility.

We hypothesize that a voxel model of tree obstruction can significantly improve the accuracy of OA visibility modelling. Precise OA visibility range information is essential for OOH media mangers who are interested in obtaining the maximum advertising impact of billboards in urban areas. From a regulatory perspective, city planners focused on visual pollution monitoring (Portella 2014; Kamičaitytė-Virbašienė, Godienė, Kavoliūnas, 2015, Chmielewski et al. 2016) also wish to know OA visibility ranges.

We first present a background on visibility analysis, elaborating on the purpose of OA visibility modelling and discussing the strengths and weaknesses of various modelling approaches. We also present a short overview of voxelization methodologies (section 2). Our results answer two essential questions: 1) What is the optimal ALS point cloud post-spacing distance for accurate 3D visibility modelling using voxelized vegetation obstruction models? And 2) what is the most optimal voxel size (volume) for this kind analysis?

We believe that these results will be helpful for other researchers deciding on the right voxel volume for their analysis, as well as on ALS point cloud thinning methods. Our workflow is dedicated to model the visibility area of a comparatively small object like advertisement billboards.

2. Existing approaches to visibility analysis

Visibility analysis, in recent decades often conducted using GIS software, has a far longer history than digital computing. A 17^{th} century military map of lines of sight and effective ranges for artillery batteries by Prestre de Vauban (1633-1707) is as an early example of spatial visibility analysis (Caldwell, 2004). Early computer based visibility analyses were conducted by Amidon & Elsner (1968); Travis, Iverson, Gary & Johnson (1975) and Felleman (1979). Among contemporary analyses several different GIS-based approaches can be distinguished, but the basic goal of these analyses is similar: to determine if the line of sight (LoS) between the observer and the target is being obstructed or not. In a brief review of different approaches to visibility modelling we will demonstrate that this assumption can be achieved in a variety of ways. Tracking the evolution from 2D to 3D, and discussing technical abilities (Table 1), we will reveal that OA visibility modelling is often still challenging in GIS environment.

Table.1 Chronological overview on different visibility modelling methods with pointed out key function abilities.

	Visibility method	Authors	Objectives						
			Dimension	Voxel based	Visible area	Visible volume of space	Visible building facade	Visibility through vegetation	Fuzzy meaner
1.	2D visibility	Amidon & Elsner (1968); Travis et al. (1975).	2D	No	Yes	No	No	No	No
2.	2D Isovist	Tandy (1967); Benedikt 1979; Hillier 1999; Batty (2001); Turner, (2001).	2D	No	Yes	No	No	No	No
3.	2D viewshed	Felleman (1979); Van den Berg et al. (1985); Shaw (1993); Cohen-Or & Shaked (1995); Wang et al. (1996, 2000); Lake (1998); Oda et al. (2000); Batty (2001); Turner (2001); Bishop & Miller (2007); Van Horn & Mosurinjohn (2010); Chamberlain & Meitner (2013); Kloucek et al. (2015).	2D	No	Yes	No	No	No	No
4.	Fuzzy & Cumulative viewshed	Higuchi (1983); Fisher (1992, 1994); Wheatley (1995); Fels (1992); Wheatley & Gillings (2000); Ogburn (2006); Rasova et al. (2013); Cahl & Rasova (2015).	2D	No	Yes	No	No	No	Yes
5.	Viewshed permeability	Dean 1997.	2D	No	Yes	No	No	Yes	Yes
6.	Visual exposure	Llobera (2003).	2D	No	Yes	No	No	Yes	Yes
7.	Probabilistic LoS	Baer et al. (2005).	2.5D	Yes	Yes	No	Yes	Yes	No
8.	Viewsphere	Yang et al. (2007).	3D	No	Yes	Yes	No	No	Yes
9.	Viewshed on voxel model	Pyysalo et al. (2009).	3D	Yes	Yes	Yes	Not tested	Yes	No
10.	3D Isovist	Morello & Ratti (2009).	3D	Yes	Yes	Yes	Not tested	No	Yes
11.	3D Isovist - Advanced Spatial Openness Index	Fisher-Gewirtzman et al. (2012; 2013).	3D	Yes	Yes	Yes	Yes	Yes[1]	Yes
12.	Visual exposure	Bartie et al. (2010, 2011, 2016).	2.5D[2]	No	Yes	No	Yes	Yes	Yes
13.	LoS & voxelized scene	Hagstrom & Messiner 2011.	3D	Yes	Yes	Not tested	Yes	Yes	Yes[3]
14.	3D visibility (ray casting)	Koltasova et al. (2013).	3D	No	Yes	No[4]	Yes	Not tested	Yes
15.	3D vector visibility	Suleiman et al. (2013).	3D	No	Yes	Not tested	Yes	Not tested	Yes
16.	3D viewshed (vertex shader)	Feng et al. (2015).	3D	No	Yes	No	Yes	Yes	No

[1] – single tree test; [2] – LiDAR based; [3] – areas of visibility uncertainty; 4 – Rhino & Grasshopper software had been used in this study, from technical point of view this software can also calculate visible volume of space with the use of voxels.

2.1 2D visibility

The most basic 2D visibility analysis is isovist, defined as a region of space, precisely a set of points, visible from a given vantage point (Tandy, 1967; Benedikt, 1979) or, alternatively, as the area not included in the shadow cast from a point light source (Morello & Ratti 2009). Isovist is dedicated to urban analysis and space-syntax cognition research (Batty, 2001a; Hillier, 1999) and gave rise to the visibility graph concept (Turner, Doxa, O'Sullivan & Penn, 2001; Conroy-Dalton & Bafna, 2003; Barthelemy, 2011; Natapov, Czamanski, & Fisher-Gewirtzman, 2013; Natapov & Fisher-Gewirtzman, 2016). 2D isovist (and related methods) is greatly challenged by 3D environments because it does not take into account either the vertical dimension (Suleiman, Joliveau, & Favier, 2011) or dynamic participants moving through space (Morello & Ratti 2009). To some measure this can be overcame by 2D viewshed which deal with non-flat areas and, to a certain extent, vegetation layers.

2D viewshed visibility is a raster-based analysis became one of the most commonly used GIS analyses for military (Van Horn & Mosurinjohn, 2010; Cohen-Or & Shaked, 1995), geography (Shaw, 1993), landscape architecture (Felleman, 1997), archaeology (Lake, Woodman, & Mithen, 1998), GSM tower (Oda, Tsunekawa & Hata, 2000), observation tower (Chamberlain & Meitner, 2013), wind farm development planning (Bishop & Miller, 2007), and urban planning visibility applications (Batty, 2001b; Turner et al. 2001). The output of 2D viewshed is a raster layer with Boolean value depicting that a pixel is either visible (1) or obscured (0). Fisher (1992) introduced fuzzy viewshed, which, after considering the probabilities of DEM errors, was modified into probable visibility (Fisher, 1994, Wu, Li & Huang 2008, Charrier & Liharrier 2012). This non-boolean, distance-dependent method asses the changing visibility of an object due to its size and distance from observer. Recently, the method was modified by Ogburn (2006) who proposed fuzzy membership to underline a distance decay visibility phenomena designed for archaeological landscapes. Similar methods for modelling visibility were also presented by Higuchi (1983) and Wheatley & Gillings

(2000), and in general there has been a trend in 2D and 3D visibility modelling literature to move towards understanding visibility as a non-binary phenomenon.

The additional factors incorporated into 2D viewshed enable analysts to understand how well a point of interest is visible from a point in a more realistic, non-Boolean manner (Nutsford, Reitsma, Pearson & Kingham, 2015; Caha & Rasova, 2015). For that reason 2D viewshed can be successfully used for OA visibility modelling, but only if distance and vegetation layers are incorporated into visibility calculations. Modern desktop GIS software (e.g. ArcGIS, FuzzyViewshed ArcToolbox, Rasova, 2013) facilitates the rapid calculation of fuzzy membership or fuzzy layer overlays that allow users to derive probabilistic cartographic representation of visibility ranges. However, so far the fuzzy approach has not applied to the OA visibility modelling. In our study a non-binary approach is proposed, with the value range corresponding to the probability of advertisement billboard visibility.

Considering the approaches of determining viewshed, raster-based viewshed should generally be regarded as a 2D analysis. Some clarification is required, then, with regard to Conroy-Dalton et al. (2003) who classified viewshed as 3D analysis. Following Biljecki et al. 2015 who has pointed out the confusing usage of "3D GIS" terminology, we argue that raster-based viewshed is 2D, however for the purpose of visualization it can be draped on a digital terrain model (DTM) or DSM to create 2.5D visualizations which may give the impression of a 3D view. The visibility analysis when using a DSM may be regarded as a 2.5D problem, if only a difference between terrain and surface elevation is taken into account. As proven by Bartie et al. (2010, 2011) a LiDAR based DSM can improve 2.5D visibility analysis and overcome two main limitations of 2D solutions: visibility through vegetation and visibility of building facades. Moreover, the most recent Bartie's & Mackaness (2016) *visual magnitude* method is capable to measure the field of view occupied by an object in the user's view, this reflect the amount seen of a target rather than the view of the surrounding spaces what is typical for its predecessors.

2.2 3D visibility

Virtual 3D – landscape visualization (Yang, 2016) and 3D visibility analysis are based on 3D features that represent the complex character of visibility obstacles. In the most basic scenario, buildings footprints can be extruded on top of a DTM to create a simple 3D representation of a landscape. Such approach is then a basis for the development of new visibility analysis that are often based on existing 2D methods. For example, isovist was modified to operate in three dimensions by the use of Spatial Openness Index (Fisher-Gewirtzman & Wagner 2003, 2006). In the extended version the isovist approach is capable to model the volume of visible space (Yang et al. 2007; Morello & Ratti, 2009) and to represent the environment regarding built-up structure, surrounding vegetation, natural light, and view (Fisher-Gewirtzman et al. 2012; 2013). The 3D version of the viewshed approach is based on voxels or 3D vectors.

A voxel (volumetric pixel or volumetric picture element) is a three-dimensional analogue of a pixel. With the use of voxelized lidar point clouds, Pyysallo et al. (2009) incorporated 3D building and vegetation obstacles into viewshed modelling. Following this path, Hagstrom & Messiner (2011) investigated the influence of the amount of unsampled voxels on 3D viewshed accuracy. Authors defined the main sources of errors in 3D visibility modelling to be irregular distribution of lidar returns. Terrain objects may be also represented with 3D vectors (Suleiman et al. 2013). By constructing 3D polygons depicting visibility obstacles, authors designed an algorithm for 3D intervisibility calculation with fuzzy results presentation. They also suggested that adjustable observer height (from human eye typical elevation 1.6 m to 2.5 m) may be useful for modelling the visibility of advertisement

billboard. Similar suggestion was also raised by Koltsova, Tunçer, & Schmitt, (2013) in the context of visual pollution modelling. However, no study confirmed the usefulness and accuracy of 3D visibility analysis to the close range visibility modelling of advertisement billboards.

2.3 LoS tracking beneath and through tree branches

The need for LoS tracking through tree branches was initially raised by Dean (1997) who proposed *viewshed permeability* concept. Later Baer W., Baer N., Powell, & Zografos (2005) presented an advanced algorithm for calculating LoS probabilities which accounts for elevation measurement errors and varying vegetation density along the LoS path. By introducing the LoS undercut index they defined the height of a clear area under tree branches through which visual signals can propagate. The index was later expanded by adding the component describing the through canopy *visual exposure* (Bartie et al. 2011). Because the LoS is influenced by the state of vegetation at different times of the year (Dachsbacher, 2011), Bartie et al. (2011) introduced a visual permeability (coverage index) of a tree canopy, to express the current LoS status along a visibility path. While rays pass through vegetated zones their rate is reduced as a function of vegetated cell permeability values.

In a 3D visibility analysis a voxelized model of vegetation can be successfully used for tracking LoS (Table 1). As an example of voxel-based visibility analysis, the visible area can be related to differences in voxel volume of terrain features (Pyysalo et al. 2009), however defining the optimal voxel size is a crucial component of the analysis. Fisher-Gewitrtzman et al. (2013) discussed the impact of vegetation on visibility by comparing analysis results with and without voxelized vegetation. Hagstorm & Messinger (2011) proved that the volume of the voxelized terrain objects affects visibility, and analysed which areas may be visible depending on the occlusion in unsampled regions. On the other hand, Feng et al. (2015) without using voxels (video games based vertex shader algorithm) successfully modelled 3D visibility beneath tree branches. Should be noted it was achieved with the use of 3D tree symbols (Fig. 1a), so raised in our study question about optimal voxels volume and sampling still needs to be answered.

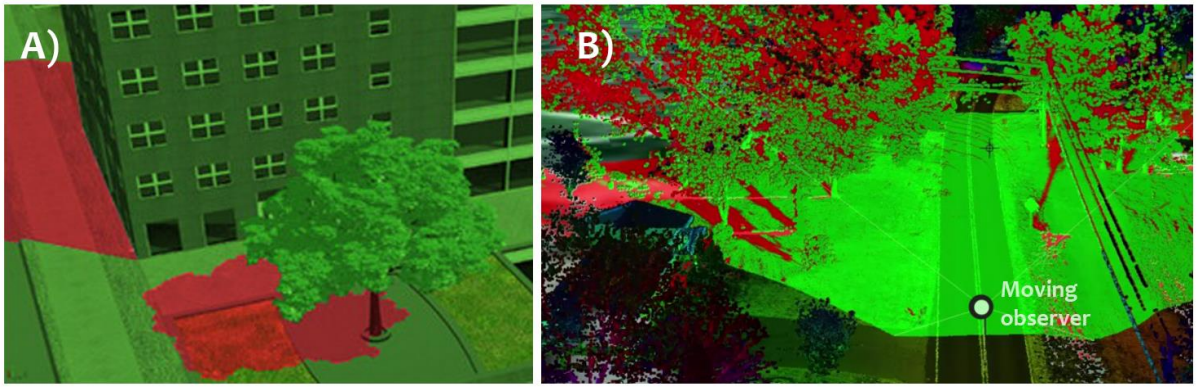

Fig. 1. Two examples of GPU-based 3D viewshed enabled to track LoS beneath tree branches: a) screenshots of the visibility analysis in GeoBeans3D. The red areas are invisible, and green areas are visible (source: Feng, et al. 2015); b) Geomedia 3D viewshed calculated on a point cloud (source: Geomedia Hexagon Group portfolio, 2016).

2.4 Voxelization and data thinning

Our methods are linked to Pyysalo et al. (2009) through our use of varying voxel volume results to differentiate the area of visibility, however we also conduct an accuracy assessment to assess the efficacy of our methods and to make our results more comparable to others in the future. Regardless of the voxelization technique applied, this kind of 3D data, along with the Bartie (2011) model, makes it possible to track LoS beneath a tree canopy and estimate the visible area of 3D cityscape features.

Here it might be prudent to ask whether it is necessary to voxelize the entire visualization environment to track LoS under a tree canopy? Hagstrom et al. (2014), Bremer et al. (2016) suggest that hybrid approaches are possible which, for example, use surfaces to define ground and voxels to define a tree canopy. Such an approach can be fruitful because surface-based raster models yield improved ground representations that lack the stair-step artefacts introduced by voxelization. Accordingly, we implement a hybrid model where ground and buildings are modelled by rasters while high vegetation and other vertical elements are modelled by voxels. This kind of hybrid model reduces computation time and utilizes the advantages of both raster and voxel data.

Because ALS-derived voxels play such a significant role in this study we describe them in a separate section below (2.4) where we conduct a short overview of ALS data voxelization and voxel-based visibility approaches in various software packages (section 2.5). We explain the differences between various voxel models, answer the question of why ALS data should be thinned before conversion into cubic voxels, and justify our use of the point instead

While the point cloud voxelization remains a simple processing task, it was proven that irregularities in point distribution due to overlap may influence the visibility analysis (Peters, Ledoux, & Biljecki 2015). Therefore, a point distribution needs to be spatially normalized before converting into voxel space (Murgoitio et al. 2013, 2014). Such normalization is achieved by performing data thinning – by reducing the number of points to some defined density, spatial distribution of points becomes more uniform. In the simplest variant, point cloud thinning is performed by overlaying a grid of defined size (e.g. 1 x 1 m) and then preserving specified number of randomly select points inside each grid cell.

Less attention has been paid to investigating how ALS thinning influences the accuracy of voxel-based visibility analysis. Using DSM accuracy assessment research as an analogue, Ruiz, Hermosilla, Mauro & Godino, (2014); Jakubowski et al. (2013) and Raber et al. (2007) all proved that extremely high ALS pulse density, as well as high point density (Pirotti &Tarolli 2010; Olsen, Puetz, & Anderson, 2009) are not necessary to acquire accurate output layers. While lidar data thinning methods are quite well described in the literature (Chu, Chen, Tseng & Wang, 2014; Guo, Wenkai, Hong, & Otto, 2010; Chow & Hodgson 2009; Gobakken & Naesset 2008; Liu, Zhang, Peterson, & Chandra 2007), a discussion on appropriate voxel volumes is present in only a few works. This absence was also pointed out by Béland et al. (2014). In their early works on savanna trees leaf area distribution (Béland et al. 2011) a general assumption was accepted that a voxel's size should be a balance between being large enough to ensure the random distribution of small scatterers, and small enough to enable the accurate identification of occluded areas and to account for foliage clumping. Additional research by Béland et al. (2014) allowed the author to propose three optimal voxel volumes for estimating the spatial distribution of within-crown leaf area density. Béland (2014) used TLS data, so the author's specific results cannot be strictly applied ALS-based voxels, however that does not change the fact that voxel volumes are a key source of variation among visualization analyses.

2.5 Software for 3D visibility

The variety of visual exposure and visibility obstacles modeling approaches are computed in a spectrum of software, mostly designed and scripted in a programming language by authors (e.g. Bartie et al. 2010, 2011) and very rarely available as open source plugins among GIS users (e.g. Rasova et al. 2013). In fact, only some are using desktop GIS software (e.g. Wrożyński et al. 2016) in favour of numerical computing software like Matlab (e.g. Pyysalo, et al. 2009; Morello & Ratti; Suleiman et al. 2013; Fisher-Gewirtzman et al. 2013; Hagstrom et al. 2014) or parametrical modelling software like Rhino with graphical algorithm editor Grasshopper (e.g. Koltsova, et al. 2013) with authors` algorithms for voxelizations (Nourian et al. 2016). The most of GIS software implementations of line-of-sight mapping rely on surface representations of a scene and can lead to erroneous results (Hagstrom & Messinger, 2012) typical for 2D visibility. This can be overcome with the use of recent 3D frustum-based algorithm (Fig. 1b) where both horizontal and vertical fields of view can be defined. Perhaps more importantly, Geoweb3d software leverages the latest advantages in Graphics Processing Units (GPU) which enables it to implement an extremely fast real-time 3D viewshed algorithm. Axell & Fridén (2015) showed that this kind of GPU implementation for a 3D viewshed can increase computation times by a factor of 3 and Ferreira et al. (2014) reported computational improvements up to the factor of 3.9. The concept of a parallel GPU-based algorithm in viewshed modeling was described, among others, by Chao, Zhuo, Xiaojing & Hantao (2011), but also Gao et al. (2011); Zhao, Padmanabhan & Wang (2012). In more recent work on GPU applications to viewshed modeling, Feng et al. (2015) reported increased 3D viewshed accuracy when only detailed 3D objects were incorporated into a 3D environment. The attached screenshot from Feng et al. (2015) (Fig. 1a) shows that this algorithm can model binary visibility beneath tree branches, an impossible task when using traditional raster-based viewshed models. The task of modeling visibility under tree branches was also the starting point for our research, with the importance of achieving this goal described in section 2.3.

3. Methods

This section describes the implementation and testing method of LoS visibility that incorporates a set of voxelized visibility obstructions. A number of processes are described and presented (Fig. 2) to give overview of the experiment workflow.

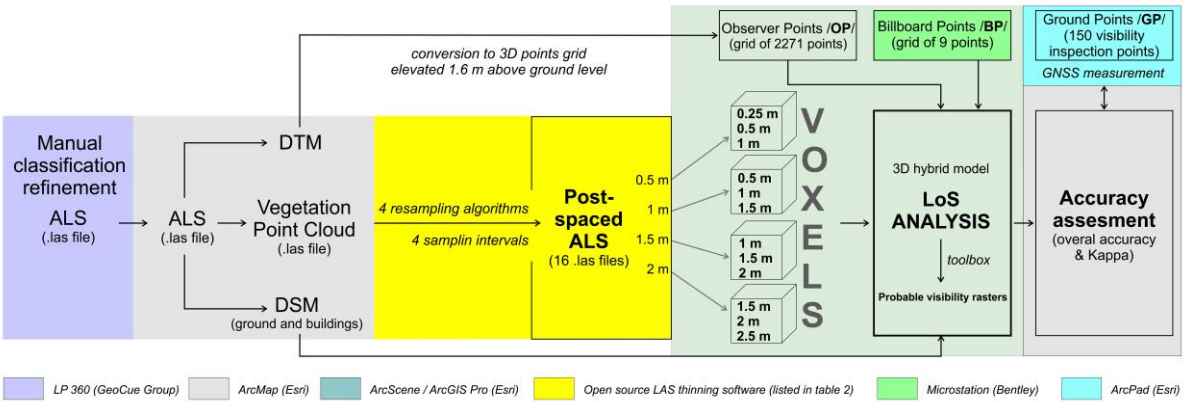

Fig. 2. Flowchart of ALS data processing and 3D visibility modelling.

Our starting point was the ALS data processing and validation, to make sure that lidar vegetation points are classified correctly. Next, extracted from lidar datasets vegetation layer was resampled with the use of several thinning algorithms (section 3.2) and finally converted

into voxels in ArcScene environment (section 3.3) where LoS analysis has been conducted (section 3.5). The accuracy assessment tolls applied in ArcMap Spatial Analyst Toolbox has been used to assess the level of accuracy of OA visibility model (section 3.6) with the reference to ground truth data recorded during field works (section 3.4).

3.1 ALS data processing

The ALS data was acquired in 2015 (leaf-on conditions), with 0.176 m post-spacing and a point density of 35.08 points/m^2, and was delivered as a classified .las file (LAS 1.2 standard). Additional manual reclassification (LP 360 software) was executed by the authors to correct any classification errors and merge high and medium vegetation into a new class called, simply, vegetation. Finally, the point cloud was classified into ground, vegetation, buildings, and other. Using ground and building classes a DSM raster was generated with a resolution of 0.5 m. This modified version of a DSM layer was later used in the hybrid voxel-raster environment, where vegetation was represented by voxels, and buildings and terrain surface were represented with the DSM.

3.2 Point cloud thinning

Point cloud thinning was performed using four algorithms implemented in three open source software packages: Meshlab (Institute of the National Research Council of Italy), 3DForest (VUKOZ Research Institute) and LAStools (Rapidlasso GmbH) (Table. 2). By defining the thinning interval we specify granularity of the grid that the LiDAR points are thinned with; the higher value of interval the less dense subsampled dataset.

Because a single lidar pulse can result in several echoes, the thinned ALS data density may be reported in two ways: as a *pulse density*, where only first return echoes are taken into account (a common specification when ordering lidar), or as a *point density* defined as number of points (all echoes) per square unit area and is commonly used to describe a point cloud dataset. The point cloud dataset is alternatively described by *point spacing* parameters given as linear units per point; after resampling (e.g. thinning) the linear units per point of subsampled dataset is reported as *post-spacing*.

Tab. 2. Thinning tools used in presented study.

Software [tool name]	Resampling method	Description
Meshlb [Sampling]	Poisson Disc Sampling	Voxels are generated according *to Poisson Disc Sampling* described by Corsini et al. (2012).
3DForest [Voxelize Cloud]	Voxel Grid Filtering	The PCL Octree algorithm, provides tree-based structure for searching, organizing and partitioning sparse 3D data.
LAStools [lasthin]	Random with *central* option OFF	A uniform grid is overlaid and a single random point is kept within each grid cell.
LAStools [lasthin – central]	Random with *central* option ON	As above; keeps the point that is closest to the centre of each grid cell.

The input vegetation-only point cloud spacing was 0.2 m (total 1162313 points). For the purpose of this study four main post-spacing intervals were implemented: 0.5 m, 1 m, 1.5 m, and 2.0 m. During resampling thinning interval values were adjusted to obtain the expected post-spacing results and to provide consistent point density among resampled datasets. Ranking the credibility of the visibility models required a similar number of points compared to voxel models. The resampled datasets were used in a hybrid voxel-raster model representing the study area.

The combination of 4 thinning algorithms and 4 post-spacing values yielded 16 downsampled point clouds.

3.3 Voxel generation

The lidar pulse occlusion and irregular sampling effects are critical issues in voxel size generation (Beland et al. 2014; Hagstrom & Messinger, 2011), especially in the case of ALS. In our experiment, we assume that interdependent ALS point cloud post-spacing and voxel sizes adjustment solves these two problems to provide sufficient visibility accuracy level without consuming computation power. To establish the relationship between voxel size and visibility accuracy for each of the post-spacing intervals, three sizes of voxels were generated: smaller, equal, and larger than post-spacing. Following Hagstrom & Messinger (2011) who used voxel sizes between 0.5 m and 2 m, in our experiment the voxel size were set to: 0.25, 0.5, 1, 1.5, and 2.0 m. For example, with point cloud post-spacing value of 1 m, the voxels size variants were set to 0.5 m (smaller), 1.0 m (equal), and 1.5 m (larger). This scheme is applied for other point-spacing and voxel size combinations, with three variants of voxel size for every point spacing value. With the use of 16 downsampled point clouds 48 individual voxelized obstruction model were created.

3.4 Field experiment design

The study was carried out in Lublin, Poland. Potential study areas were limited to places where dense, high vegetation and standard sized OA were both present. For the purpose of this study a single-sided 6 x 3 m OA board located near a city park (*Academic Park* in Lublin) was selected. The OA stands on a 3.5 m pylon with its upper edge elevated 6.5 m above ground level.

The study area (8.8 ha) is relatively hilly, elevated from 193 m to 212.8 m a s.l., in 45.4% covered by mixed high vegetation; 30,6% by low and medium vegetation; 9,7 % by buildings and 14,3 by roads and pathways. The exact OA location was acquired with the use of a GNSS-RTK receiver coupled with a laser rangefinder (TP-360B) to describe the 3D location of the OA board. Next, with the use of CAD software (Microstation V8i) a 3D vector model of the OA board was created. The surface of the OA board was divided into 9 equal 1 x 2 m rectangles, each with a centroid referred to as a board point (BP). Finally in our experiment, the OA board was represented by the grid of nine BPs.

Similar to Kloucek et al. (2015), the field experimental design was based on a reference model consisting of 150 ground truth visibility points (GPs) (Fig. 3). The location of GPs was randomized with some exceptions. Because this research is focused on OOH media visibility, we determined that visibility should be considered mainly near pedestrian and vehicle traffic areas where OA media are most likely to be witnessed. GPs were set up within 200 m and a 160° field of view from the OA board, i.e. within the typical readability range for 6x3m OA (Chmielewski et. al 2016). Points that fell in hazardous places (e.g. the pedestrian and car traffic intersections) were shifted. Next, the GPs has been copied to the GNSS computer memory to make able the field crew to navigate to the exact location of GP. From each GP a photograph of the OA was taken, and was further (office works) overlaid

with a grid of 9 BPs (Fig. 4) in graphic computer software. Then, with the use of this images, a level of OA board visibility (LOV) was determined at each of the points based on the number of visible BPs. The unobstructed points were then counted and the LOV recorded using a 9-point scale ranging from 9 (full visible) to 0 (not visible) according to the number of unobstructed BPs (a GIS simulation of this process is presented in Fig. 5). Finally, the LOV reflect the unobstructed part of OA visible from each of GPs.

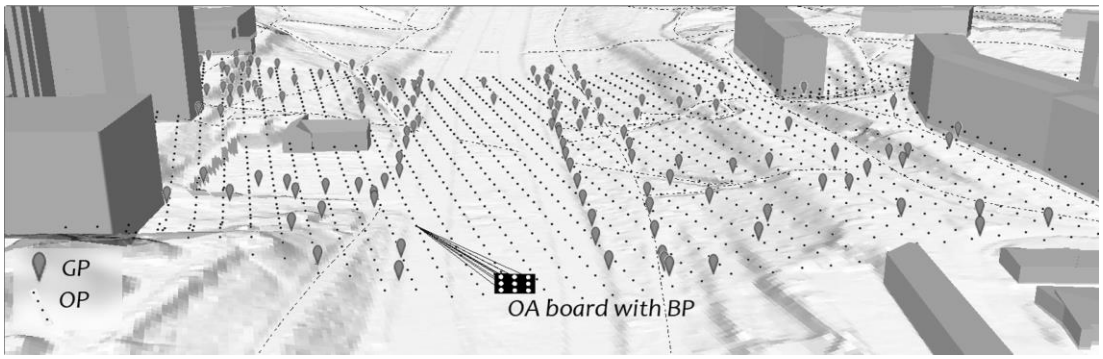

Fig. 3. Field experimental design - the distribution of 150 ground truth visibility control points (150 GPs, grey pushpins) and 2271 observation points (2271 OPs, black dots) elevated 1.6 m above ground level. A single LoS from an example of single OP is also presented to explain how LoS are constructed between OPs and GPs (the vegetation layer was removed to provide clarity).

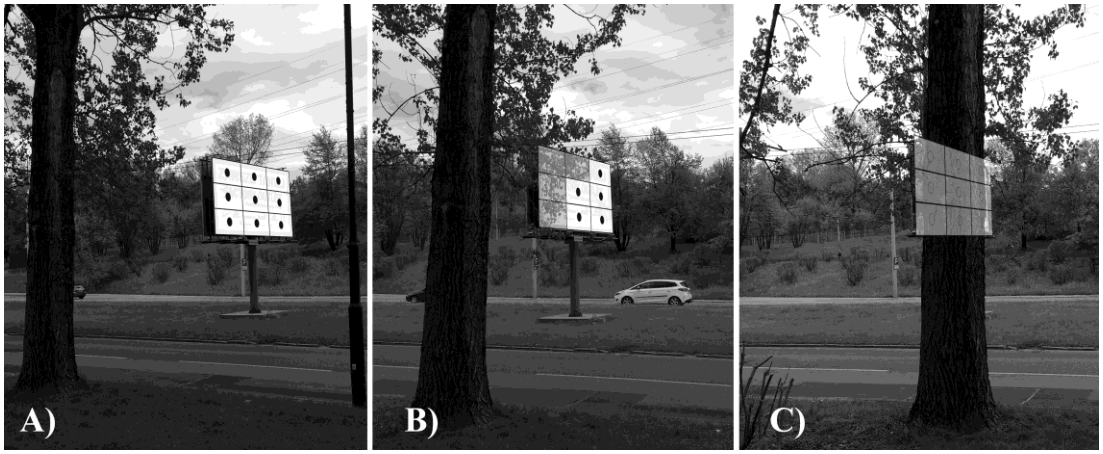

Fig. 4. Photo-based simulation of an OA board obscured by virtual vegetation: (A) entire OA visible, (B) OA board partially covered, (C) OA board entirely invisible.

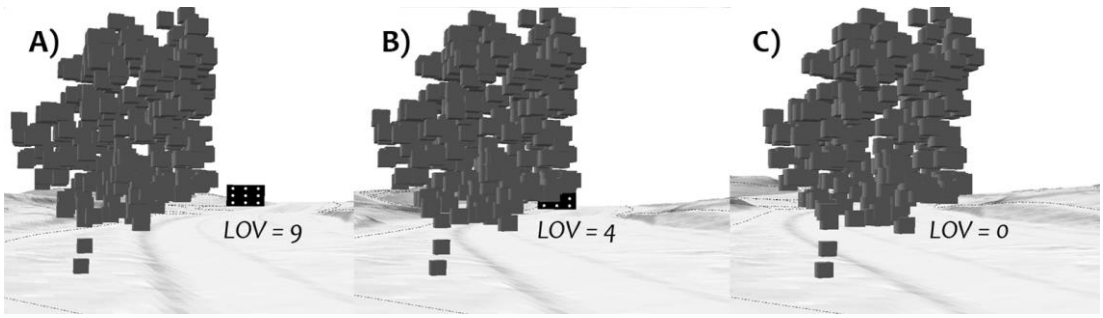

Fig. 5. 3D simulation of an OA board obscured by voxelized vegetation: (A) entire OA visible, (B) OA board partially covered by vegetation, (C) OA board entirely invisible.

To provide an equal proportion between visible (LOV = 9), covered (LOV ÷ 1-8) and invisible (LOV = 0) GPs, an additional set of 50 GPs was also added in "sensitive" locations. The 150 GPs were suspended at the average human eye height of 1.6 m above the ground level (Schirpke, Tasser & Tappeiner, 2013, Kułaga et al. 2011). Exact point locations were established using GNSS and the LOV was then estimated at each GP.

3.5 Visibility Analysis

The visibility of the OA board was analysed with the use of LoS between the observation points (OPs) and the BPs. OPs were established as a 5 m sampled point grid elevated 1.6 m above ground level. In total 2271 OPs were used. The OP sampling distance is a function of the expected output layer's resolution – we used 5 m spacing as it is sufficient for detailed OA visibility analyses.

At each OP the number of visible BPs was determined. During LoS visibility analysis three kinds of visual obstructions were taken into account: ground surface, buildings (both represented by raster models) and high and medium vegetation (represented by the voxelized point cloud). LoS analysis resulted in target visibility lines (tVL) by counting tVL a LOV value was assigned to each OP. To automatically process this task a simple geoprocessing tool (Model Builder) was designed (Fig. 6).

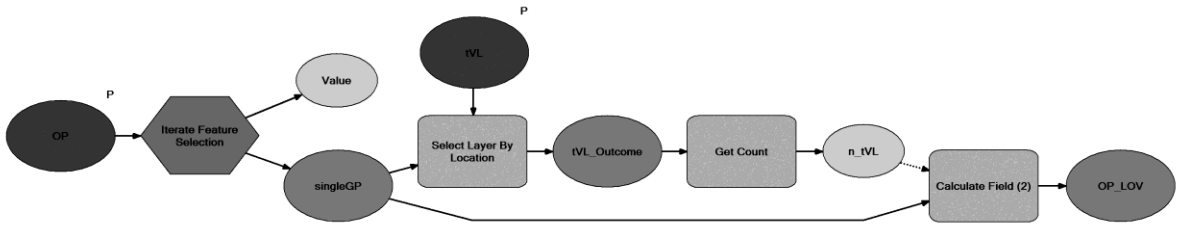

Fig. 6. Geoprocessing tool that assigns LOV value to the OP. First, a single OP is iterated. Next the number of tVL for this point are counted. Finally, this number is assigned back to the OP in a new field called LOV.

As LOV values were assigned as an attribute of OPs, a 5 m GSD Visibility Raster (VR) was generated by LOV value field. For 3D visualization, the VR was displayed using a colour ramp (from blue to red) to show the level of OA board visibility as a continuous variable (as was simulated in Fig. 3). Additionally, to assess the degree to which a voxelized point cloud improves the level of visibility model accuracy, we calculated a 2D cumulative viewshed (for all BPs) and an accuracy assessment was performed in a similar manner to the LoS approach.

3.6. Statistical analysis and error estimation

For each of the visibility models an overall accuracy (OAc) and Kappa were calculated based on an error matrix. Because the geoprocessing tool recorded only the number of visible BPs and not the ID of each of visible BP, a VR reclassification was performed using three classes: visible (VR = 9 reclassified to 2); partially visible (VR from 1 to 8 reclassified to 1) and not-visible (VR = 0 stays as 0). The GPs were reclassified with the same scheme. Finally, the VR accuracy assessment was conducted using the "visible", "partially visible" and "not visible" classes.

4. Results

4.1. ALS thinning results

The detailed statistics of the downsampled point clouds are given in section A of table 3. By adjustments of the sampling interval parameter, expected post-spacing intervals were achieved with the use of various thinning algorithms. Despite this, individual point cloud datasets differed slightly in their total point counts. The most significant differences for 0.5 m, 1 m, 1.5 m and 2.0 m post-spacing were 17 182 points (9,7%); 3 744 points (8.6%) 6 377 points (33,7%) and 4 296 points (61.45) respectively. These differences arose from different point cloud filtering schemes implemented in the software tools. They lose importance as the point density parameter is taken into account, and we only noted the 8.1% density difference for the 0.5 m post-spacing and 28.6% density difference for the 2 m post-spacing. For the voxel creation process, the spaces between points are occupied by the exact voxel volume, therefore the post-spacing parameter becomes very important. Because of a the multitude (48) of obstructions models generate, only a single example is presented in Fig. 7 to visualize the influence of various voxel sizes and post-spacing on the resolution of vegetation visibility obstructions model.

Table. 3. Section A: statistics for the resampled vegetation layer point cloud (visibility obstruction). Section B: 3D visibility model errors with computation times.

	Section A					Section B Overall Accuracy (%) Kappa (%) Computation Time (hours; minutes)					
Software	Point Cloud No	Sampling interval	Post-spacing	Number of points	Points density	voxel 0.25 m	voxel 0.5 m	voxel 1 m	voxel 1.5 m	voxel 2 m	voxel 2.5 m
3D forest (Voxel Grid Filtering)	1	1.2 m	0.5 m	159 795	3.73	OAc 57.3 K 37.7 T 7;51	OAc 70 K 54,5 T 7;54	OAc 65.3 K 45.5 T 7;26			
	2	2.33 m	1 m	39 604	1.00		OAc 52.7 K 30.9 T 2;26	OAc 74 K 60.2 T 2;41	OAc 64 K 43.1 T 2;29		
	3	3.90 m	1.5 m	12 521	0.44			OAc 57,3 K 36,7 T 0;51	OAc 64.7 K 46.1 T 0;52	OAc 60.7 K 38.4 T 0;52	
	4	5.12 m	2 m	6861	0.35				OAc 60.0 K 40.0 T 0;43	OAc 61.3 K 39.3 T 0;44	OAc 57.3 K 32.5 T 0;42
Meshlab (Poisson Disc Samping)	5	0.8 m	0.5 m	176 977	4.06	OAc 51.3 K 28.4 T 14;10	OAc 70.7 K 55.4 T 14;6	OAc 64.7 K 44,4 T 14;16			
	6	1.71	1 m	41 159	1		OAc 54.7 K 33.8 T 8;30	OAc 70.7 K 55.0 T 8;35	OAc 64.0 K 42.8 T 8;39		
	7	2.75 m	1.5 m	14 467	0.44			OAc 60.7 K 41.7 T 1;31	OAc 61.3 K 40.7 T 1;28	OAc 58.0 K 33.4 T 1;32	
	8	3.77	2m	6849	0.32				OAc 62.6 K 44.0 T 0;45	OAc 60.0 K 38.2 T 0;46	OAc 58.0 K 32.8 T 0;47
LasTools (random)	9	0.44 m	0.5 m	174 196	3.94	OAc 56.0 K 35.7 T 9;18	OAc 64.7 K 46.7 T 9;12	OAc 69.3 K 52.6 T 9;19			
	10	0.951 m	1 m	42 575	1		OAc 52.7 K 31.1 T 2;28	OAc 65.3 K 47.4 T 2;25	OAc 68.7 K 51.7 T 2;30		
	11	1.57 m	1.5 m	17 326	0.45			OAc 61.3 K 42.5 T 1;24	OAc 65.3 K 47.3 T 1;33	OAc 67.3 K 49.1 T 1;16	
	12	2.0 m	2 m	11 145	0.25				OAc 64.0 K 45.8 T 0;54	OAc 70.7 K 54.9 T 0;58	OAc 66.7 K 48.0 T 0;56
LasTools (random, centered)	13	0.44 m	0.5 m	174 196	3.94	OAc 54.0 K 32.9 T 7;30	OAc 66.7 K 50.0 T 7;30	OAc 68.7 K 51.3 T 7;21			
	14	0.94 m	1 m	43 348	1.00		OAc 65.3 K 47.5 T 2;19	OAc 64.7 K 46.4 T 2;35	OAc 70.7 K 54.7 T 3;07		
	15	1.49 m	1.5 m	18 898	0.44			OAc 66 K 54.7 T 1;16	OAc 70.7 K 55.1 T 1;18	OAc 68.7 K 51.4 T 1;15	
	16	2.0	2.0	11 145	0.25				OAc 64.7 K 46.8 T 0;57	OAc 70.7 K 54.9 T 0;56	OAc 64.7 K 44.8 T 0;59
3D LoS *No Vegetation*	-	-	-	-	-	OAc 33.3; K 10.6; T 0;08					
2D Viewshed (DSM)	-	-	-	-	-	OAc 51.3; K19.7; T 0;01					

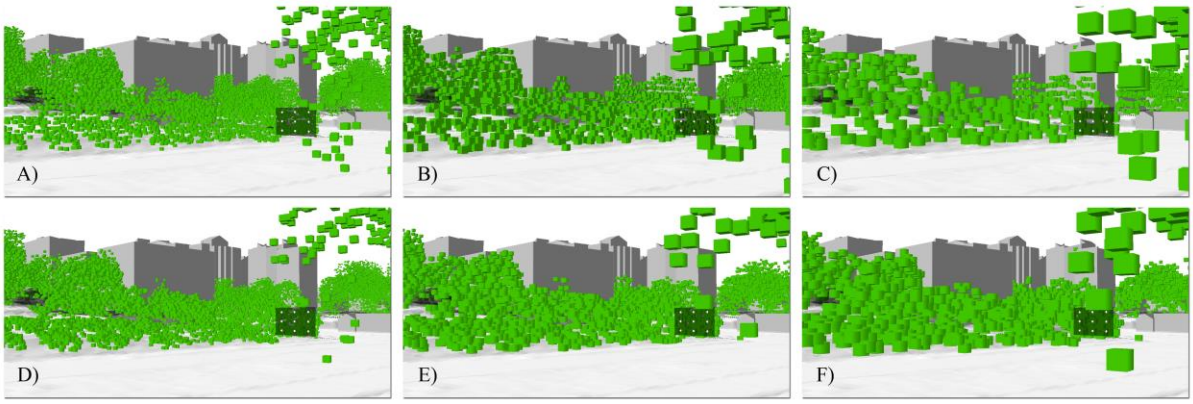

Fig. 7. Three levels of post-spacing with the use of PCL Voxel Grid Filtering (from A to C) and LasThin (from D to E). A and D post-spacing and voxel cube size = 0.5 m. B and E post-spacing and voxel cube size = 1 m. C and F post spacing and voxel cubes size = 1.5 m

4.2. The most accurate model

The results listed in section B of table 3 summarize the accuracy of the all 48 visibility models generated. An example of the error matrix used to obtain this summary is presented in

Tab. 4. Examples of error matrix used for visibility models accuracy estimation: A) the lowest accuracy, B) the highest accuracy ("*0*" – not visible; *1* – partially visible; *2* – visible; OAc – overall accuracy; K – Kappa`s coefficient).

A)

		Truth (GPs)				
		0	*1*	*2*	Total	UA
Predicted visibility	*0*	13	9	1	23	57%
	1	43	32	2	77	42%
	2	7	11	32	50	64%
	Total	63	52	35	150	
	PA	21%	62%	91%		
	OAc=51.3%; K=28.4%					

B)

		Truth (GPs)				
		0	*1*	*2*	Total	UA
Predicted visibility	*0*	47	18	0	65	72%
	1	12	30	1	43	70%
	2	4	4	34	42	81%
	Total	63	52	35	150	
	PA	75%	58%	97%		
	OAc=74%; K=60.2%					

The error matrix (also known as the confusion matrix) as established method of land cover classification results accuracy assessment in remote sensing studies (e.g. Chakraborty, Sachdeva & Joshi, 2016). In our case study it has been applied to rapport the accuracy of 3D visibility model. The error matrix is calculated with reference to ground truth visibility validated during field works in 150 GPs; the 3D visibility model is treated as *predicted* values. The overall accuracy (OAc) reflect the percentage of *predicted* that meets the *truth*. The Kappa`s coefficient measure of how the visibility results compare to values assigned by chance; a Kappa of 0 indicates agreement equivalent to chance, the higher the kappa coefficient, the more accurate the classification is. Furthermore, the *producer accuracy* (*PA*) and *user accuracy* (*UA*) reflect the commission and omission errors respectively.

The most robust visibility model is achieved when vegetation is not included into the visibility environment (OAc 33.3%; K 10.6%; Table 3, section B). This model was designed purposely to show the importance of visibility obstructions created by high vegetation. The least-precise result is the 2D viewshed model (OAc 51.3%; K 10.6) where both buildings and vegetation were modelled by a high resolution raster (0.5 m GSD). As reported by Maloy & Dean (2001), as well as Kloucek et al. (2015), 2D viewshed models at some conditions can achieve accuracy above about 50%. At only 1 minute, 2D viewshed was by far the fastest-computed model, however. For the 3D LoS models, overall accuracy ranges from 51.3% to 74.0% and is confirmed by Kappa ranging from 28.4 to 60.2. Fig. 8 presents the three most

descriptive results over-visibility, where undersized voxels result in an oversized field of visibility; accurate visibility, with an optimal 1m voxel size; and under-visibility, where oversized voxels result in an undersized field of visibility. The colour ranges indicate the LOV and reveal how voxels parameters influence the visibility models, providing considerably more information than a binary visible/not visible image. It should also be noted here that visibility is being modelled beneath tree canopy.

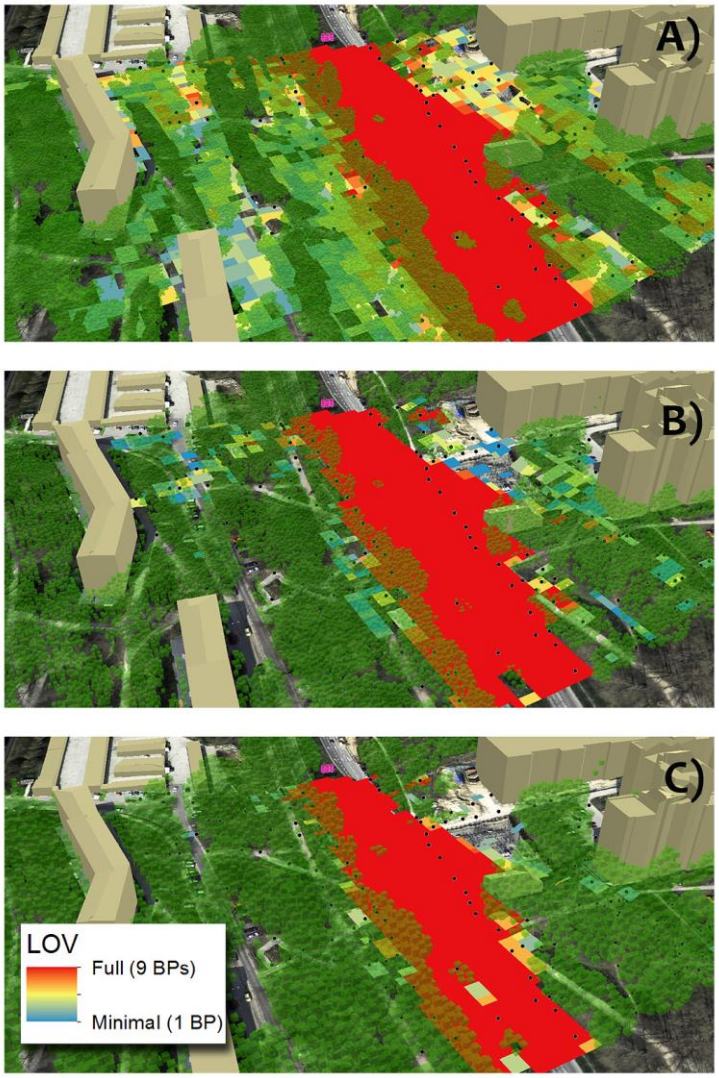

Fig. 8. The impact of post-spacing and voxel volume on visibility models: A) over-visibility effect; B) the most accurate visibility; C) under-visibility effect. The LOV is shown in a colour ramp from red (OA board fully visible) to blue (OA board almost complexly covered by visibility obstructions).

Our expectation that the highest accuracy would be achieved when post-spacing and cube size parameters were the same was largely supported, both in Voxel Grid Filtering and Poisson Disc Sampling. The most accurate model used a 1 m voxel thinned by Voxel Grid Filtering to 1m post-spacing, achieving an overall accuracy of 74% and a Kappa of 60.2%. A different output resulted from the use of Lasthinn random algorithms. Here, a cube size greater than post-spacing tends to be lead to higher accuracy (no more than 6%). At post spacing equal to 2.0 m, the visibility obstruction model created with the use of Lasthin confirmed our expectations.

As we compare the number of voxels used in each model and its level of accuracy, we see that the highest accuracy is not achieved from the densest datasets. Indeed, a sparser point

cloud (e.g. 11 145 voxels) can provide good results (OAc ~ 70%) in a short time compared to denser datasets. For example, a 176 997 voxel model with 0.5 m Poison Disc Sampling resulted in the same accuracy as the less dense point cloud, despite taking three times longer to compute.

The computation times listed in Table 3, are ranged from 14 hours and 16 minutes to 42 minutes and are directly dependent on the number of voxels in the dataset. Within one point cloud the small fluctuations in computation times appear which may be explained by the slightly decreased efficiency of the LoS algorithm when run in batch mode using ArcGIS software. The presented computation times may be helpful for other users who may want to repeat our approach to OA visibility modelling. Our pre-tests (Core i7, 16GB RAM, VGA 2GB) revealed that the ArcScene software is unable to process more than 500 000 voxels in computation times of less than 30 hours.

5. **Discussion and conclusions**

In this paper we demonstrated the influence of the point cloud post-spacing interval and its interaction with voxel size on 3D visibility modelling of OOH media. Contrary to Tan et al. (2015) who suggested that "*lower resolution is less accurate*" we demonstrate that such statement is not always correct, by investigating the accuracy of voxel-based visibility on the voxels resolution (the resolution expressed as point-spacing and voxel cubes size). Our results showed that the best results were obtained with a PCL-based Voxel Grid Filtering algorithm at 1 m post-spacing, and with 1 m voxel size. The approach presented here is novel as it incorporates the 3D properties of vegetation, resulting in an increase in the accuracy of generated lines of sight.

Beside 3D visibility studies also solar potential estimation seek for proper 3D vegetation models to be implemented into 3D applications of urban environment solar irradiation modelling. (e.g. v-sun model by Hofierka & Zlocha, 2012 in the framework of GRAS-GIS, or SVOSUN3D by Liang & Gong, 2017). In fact, Hofierka & Zlocha (2012) has been using 2.5 m voxels, Bremer et al. (2016) has generated smaller 1 m voxels, but no additional studies on voxel volume on shadow casting effect has been undertaken so fare, therefore our findings may be also useful for other, visibility related applications. Moreover, our results may be regarded as coherent with Wang, Weinacker & Koch, (2008) who has recommended voxels with horizontal resolution of 0.5 m and thickness of 1 meter as the most valuable for single tree modelling. On the other side, Sindram et al. (2016) argue that for the purpose of building volume calculation the finest voxel resolution is recommended, therefore it must be pointed out that optimal voxel volume depends on the purpose of the 3D analysis.

Our research confirms that 3D analysis can provide more accurate results than 2D analysis (Stoter et al. 2013; Herbert & Chen, 2015; Feng et al. 2015;). We have also confirmed the assumption proposed by others (Jakubowski, Guo 7 Kelly, 2013; Treitz et al. 2012; Pirotti et al. 2010; Olsen et al. 2009) that downsampled lidar data can provide comparable results to full resolution datasets, an assumption that can now be extended to visibility modelling. While earlier studies using ALS were conducted with low pulse density, possibly explained by the relatively low pulse repetition frequency of the first lidar sensors (Csanyi & Toth 2006), more recent ALS data are acquired with high pulse density, often exceeding 8 pulses/m^2 (USGS, 2014). A short overview of purpose-dependent resolution for ALS acquisition is given by the Oregon Lidar Consortium (OLC), who recommend pulse spacing ranging from 4 to 8 pulses per meter, meaning that post-spacing from 0.25 - 0.5 m may be expected by the end user of modern ALS data (OLC, 2009). The visibility analysis conducted with the use of such dense ALS data requires high computation time, this can be overcome by proper downsampling procedure with controlled loss of final model accuracy.

Our approach underlines the importance of incorporating vegetation into visibility analysis (Fisher, 1994; Bartie, Mackaness, Petrenz & Dickinson, 2015). The vegetation visibility obstruction can be modelled in 3D optimal voxel size and post-pacing parameters yielding better results than others. Contrary to Pyysallo et al. (2009) who aligned voxel volume with ALS impulse footprint size, we base our recommendations on the results of visibility accuracy levels. The Hagstrom et al. (2014) approach to the level of unsampled voxels can also be applied to estimate appropriate voxel size. More than other literature to date, we test the influence of ALS data thinning methods on voxel-based visibility. This problem has not, to our knowledge, been raised in the international literature so far and the findings may be applicable in the field of computer graphics (Dyn, Iske, & Wendland, 2008.) Our approach was executed with commonly used GIS software and other users can apply our findings with no requirement for programing skills.

Although the best thinning tools has been indicated (PCL Voxel Grid Filtering), due to similar levels of accuracy achieved in each of the post-spacing groups, we conclude that voxel cube size adjusted to post-spacing value has the primary influence on the final OA visibility model. We cannot solely recommend the PCL Voxel Grid Filtering algorithm because only 4 of many available thinning algorithms have been tested here. For the purpose of similar studies, other thinning tools available in other software packages like CloudCompare (random, space and octree subsample) or MathWorks (random or box voxel grid filtering) can be applied.

It was predictable that undersized voxels would result with over-visibility, however their utility needs to be assessed for leaf-off visibility modelling. Terrestrial Laser Scanning (TLS) can provide extremely dense point clouds to create leaf-off visibility tree models. ALS data acquired during leaf-on seasons are inadequate for these kinds of models, but at some level of thinning level the voxels could partially block visibility in a more or less comparable way to TLS-derived leaf-off models. This hypothesis requires further research to be tested.

To summarize by addressing our research questions, we may conclude the following:

1. If the accuracy of OA visibility model is expected to be higher than 50% then an ALS-derived voxelized vegetation layer should be incorporated into a 3D analysis environment.
2. Thinning methods have important secondary impacts on model accuracy. In our study the best results were achieved with the use of a PCL-based Voxel Grid Filtering algorithm
3. As an optimal post-spacing we recommend a 1 m interval, but the in case of larger research areas (with a greater number of voxels) a 1.5 or even 2.0m post spacing can be used to reduce computation times with little loss of final model accuracy. In case of highly thinned point clouds, the Lasthin algorithm may be recommended.
4. A voxel volume adjusted to the post-spacing interval provides the highest accuracy of visibility models.

Acknowledgement

The authors would like to thank the **Polish National Science** Centre (NCN), which in July 2013 decided to finance this research (DEC-2012/07/D/HS4/01569).
We also would like to thank **Jan Trochta** (VUKOZ, Department of Forest Ecology) for adopting 3DForest software for ours study. Many thanks to **Danbi Lee** (cityspatial.co) and **Dave William** (UBC, Landscape Ecology Lab.) for worthwhile suggestion during manuscript preparation.

References:

1. Amidon, E., & Elsner, G. H. (1968). Delineating Landscape View Areas: a computer approach. U.S Department of Agriculture, Washington, D.C. (pp. 1–6).
2. Axell T. & Fridén M. (2015). Comparison between GPU and parallel CPU optimizations in viewshed analysis. Master's thesis in Computer Science: Algorithms, Languages and Logic. Department of Computer Science and Engineering, Chalmers University Of Technology Gothenburg, Sweden, (pp. 1-63).
3. Baer W., Baer, N., Powell, W. & Zografos, M. (2005). Advances in terrain augmented geometric pairing algorithms for operational test. Modeling and simulation workshop, Dec. 12-15, Las Cruces, NM.
4. Barthelemy, M. (2011). Spatial networks. Physics Reports, 499, (pp. 1–101)
5. Bartie, P., Reitsma, F., Kingham, S., & Mills, S. (2010). Advancing visibility modelling algorithms for urban environments. Computers, Environment and Urban Systems, 34(6), 518–531.
6. Bartie, P., Reitsma, F., Kingham, S., & Mills, S. (2011). Incorporating vegetation into visual exposure modelling in urban environments. *International Journal of Geographical Information Science*, 5(5), 851-868.
7. Bartie P., Mackaness W., Petrenz P. & Dickinson A. (2015). Identifying related landmark tags in urban scenes using spatial and semantic clustering. *Computers, Environment and Urban Systems,* 52: 48–57.
8. Bartie, P., & Mackaness, W. (2016). Mapping the visual magnitude of popular tourist sites in Edinburgh city, *Journal of Maps, 12(2): 203-210.*
9. Batty, M. (2001a). Polynucleated urban landscapes. *Urban Studies* 38(4), 635-655.
10. Batty, M. (2001b). Exploring isovist fields: space and shape in architectural and urban morphology. *Environment and planning B: Planning and Design*, 28(1), 123-150.
11. Béland, M., Widlowski, J.-L., Fournier, R., Côté, J.-F., & Verstraete, M. M. (2011). Estimating leaf area distribution in savanna trees from terrestrial LiDAR measurements. *Agricultural and Forest Meteorology*, 151(9),1252–1266.
12. Béland, M., Baldocchia, D., D., Widlowskic, J.-L., Fournier, R., A. & Verstraetec, M., M. (2014) On seeing the wood from the leaves and the role of voxel size indetermining leaf area distribution of forests with terrestrial LiDAR. *Agricultural and Forest Meteorology*, 184, 82– 97.
13. Benedikt, M., L. (1979). To take hold of space: isovists and isovist fields, *Environment and Planning B, 6*. 47–65.
14. Biljecki, F., Stoter, J., Ledoux, H., Zlatanova, S., & Çöltekin, A. (2015). Applications of 3D City Models: State of the Art Review. ISPRS International Journal of Geo-Information, 4(4), 2842–2889
15. Bilsen, A. & Stolk, E. (2008). Solving Error Problems in Visibility Analysis for Urban Environments by Shifting from a Discrete to a Continuous Approach. *Computational Sciences and Its Applications, ICCSA International Conference on*, Perugia, (pp. 523-528).
16. Bishop, D., I. & Miller R., D. (2007). Visual Assessment of off-shore wind turbines: the Influence of distance, contrast, movement and social variables. *Renewable Energy*, 32, 814-831.
17. Brabyn, L. & Mark, D., M. (2011). Using viewsheds, GIS, and a landscape classification to tag landscape photographs. *Applied Geography*, 31: 1115-1122.
18. Brabyn, L. (2015). Modelling landscape experience using "experions". *Applied Geography*, 62: 210-216.
19. Bremer, M., Mayr, A., Wichmann, V., Schmidtner, K. & Rutzinger, M. (2016). A new multi-scale 3D-GIS-approach for the assessment and dissemination of solar income of digital city models. *Computers, Environment and Urban Systems*, 57, 144–154.
20. Caha, J. & Rasova, A. (2015). Line-of-sight derived indices: viewing angle difference to a local horizon and the difference of viewing angle and the slope of line of sight. Růžičková, K., Inspektor, T. (Eds.). Surface models for geosciences, chapter 6, Springer, (pp. 61-72).
21. Caldwell, D. (2004). Studies in military geography and geology. Dordrecht, Cluver Academic Publishers, (pp. 1-348).
22. Chamberlain, B. & Meitner, M. (2013). A route-based visibility analysis for landscape management. *Landscape and Urban Planning*, 11, 13-24.
23. Chao F, Y., Zhuo, Ch., C., Xiaojing, Y., & Hantao, G. (2011). Parallel algorithm for viewshed analysis on a modern GPU, *Int. J. Digital Earth*, 4(6), 471–486.
24. Chakraborty, A., Sachdeva, K. & Joshi, P., K. (2016). Mapping long-term land use and land cover change in the central Himalayan region using a tree-based ensemble classification approach. *Applied Geography*, 74: 136-150.
25. Charrier, R & Li, Y. (2012). Assessing resolution and source effects of digital elevation models on automated floodplain delineation: A case study from the Camp Creek Watershed, Missouri. *Applied Geography*, 34: 38-46.

26. Chmielewski, Sz., Lee, D., Tompalski, P., Chmielewski, T. & Wężyk P. (2016) Measuring visual pollution by outdoor advertisements in an urban street using intervisibility analysis and public surveys. *International Journal of Geographical Information Science*, 30(4), 801-818.
27. Chow, T., E. & Hodgson, E., M. (2009). Effects of lidar post-spacing and DEM resolution to mean slope estimation. *International Journal of Geographical Information Science*, 23(10), 1277–1295.
28. Chu, H., Chen, R., Tseng, Y. & Wang, C. (2014), Identifying LiDAR sample uncertainty on terrain features from DEM simulation, *Geomorphology*, 204, 325–333.
29. Cohen-Or, D., & Shaked, A. (1995) Visibility and dead-zones in digital terrain maps. *Eurographics Association* (14)3, 171-180.
30. Conroy-Dalton, R. & Bafna, S. (2003) The syntactical image of the city: A reciprocal definition of spatial elements and spatial syntaxes. Proceedings *4th International Space Syntax Symposium*, London, (pp: 1-22).
31. Csanyi, N. & Toth, C., K. (2006). Lidar data accuracy: the impact of pulse repetition rate. *MAPPS/ASPRS Fall Conference*, November 6 – 10, San Antonio, Texas.
32. Dachsbacher, C. (2011). Analyzing visibility configurations. *IEEE Transactions On Visualization And Computer Graphics*, 17(4) 4, 475-486.
33. Dean, D., J. (1997). Improving the accuracy of forest viewsheds using triangulated networks and the visual permeability method. *Canadian Journal of Forest Research*, 27, 969–977.
34. Dyn, N., Iske, A. & Wendland, H. (2008). Meshfree Thinning of 3D Point Clouds. *Foundations of Computational Mathematics*, 8(4), 409-425.
35. Felleman, J. (1979). Landscape visibility mapping, theory and practice, School of Landscape Architecture, SUNY, College of Environmental Science and Forestry, (pp. 1-111).
36. Felleman, J., P. (1986) Landscape visibility. In. *Foundations for visual project analysis*, Smardon, C., R., Palmer, J., F. & Felleman, J. P. (Eds.), John Wiley & Sons. NY, (pp. 307-333).
37. Feng, W., Gang, W., Deji, P., Yuan, Y., Liuzhong, Y. & Hongbo, W. (2015) A parallel algorithm for viewshed analysis in three-dimensional. *Digital Earth Computers & Geosciences*, 75, 57–65.
38. Ferreira, Ch., R., Andrade, M., V., A., Magalhães, S., V., G., Franklin, W. R. & Pena, G., C. (2014). A parallel algorithm for viewshed computation on grid terrains. *Journal of Information and Data Management*, 5(1), 1-10.
39. Fisher Gewirtzman, D. & Wagner, I. A. (2003). Spatial openness as a practical metric for evaluating built-up environments. *Environment and Planning B: Planning and Design*, 30(1), 37–49.
40. Fisher-Gewirtzman, D. & Wagner, I. A. (2006). The 'spatial openness index': an automated model for 3D visual analysis of urban environments. *Journal of Architecture and Planning Research*, 23(1), 77–89.
41. Fisher-Gewirtzman, D. (2012). 3D models as a platform for urban analysis and studies on human perception of space. *Usage, Usability, and Utility of 3D City Models*, 01001: 1-16 (DOI: 10.1051/3u3d/201201001)
42. Fisher-Gewirtzman, D., Shashkov, A. & Doytsher, Y. (2013). Voxel based volumetric visibility analysis of urban environments. *Survey Review* 45, 451–461.
43. Fisher, P.F., 1992. First experiments in viewshed uncertainty: Simulating fuzzy viewsheds. *Photogrammetric Engineering and Remote Sensing*, 58 (3), 345–352.
44. Fisher, P. F. (1994). Probable and fuzzy models of the viewshed operation. In Worboys, M. (Ed.), *Innovations in GIS*, London: Taylor & Francis, (pp. 161 – 175).
45. Gao, Y., Liu, H., Yu, Y., Liu, Y., Liu, M. & Zhao, Y. (2011) Optimization for viewshed analysis on GPU. *19th International Conference on Geoinformatics IEEE*, 24-26 June, Shanghai, (pp. 1–5).
46. Geomedia Hexagon Group portfolio (2016). *GIS/Point cloud integration*. Video source: http://www.hexagongeospatial.com/products/producer-suite/geomedia-3d. [accessed Sept. 2016].
47. Gobakken, T., & Naesset, E. (2008). Assessing effects of laser point density, ground sampling intensity, and field sample plot size on biophysical stand properties derived from airborne laser scanner data. *Canadian Journal of Forest Research*, 38(5), 1095–109.
48. Guo, Q., Wenkai, L., Hong, Y. & Otto A. (2010). Effects of Topographic Variability and Lidar Sampling Density on Several DEM Interpolation Methods. *Photogrammetric Engineering & Remote Sensing*, 76(6), 1-12.
49. Hagstrom, S. & Messinger D. (2011). Line-of-sight analysis using voxelized discrete lidar. *Proc. SPIE Laser Radar Technology and Applications XVI*, Turner, M. & Kamerman, G. (Eds.) 8037 (80370B), 1-11.
50. Hagstrom, S. & Messinger D. (2012). Line of sight measurement in large urban areas using voxelized LIDAR. Proc. of SPIE Vol. 8379: 1-12.
51. Hagstrom, S., Messinger, D & Salvaggio, K., N. (2014). Estimating sampling completeness of lidar datasets using voxel-based geometry. *Proc. SPIE* 9080-25, *Laser Radar Technology and Applications XIX; and Atmospheric Propagation XI*, June 9, Baltimore, Maryland.
52. Herbert, G.; Chen, X. (2015). A comparison of usefulness of 2D and 3D representations of urban planning. *Cartogr. Geogr. Inf. Sci.*, 42(1): 22–32.

53. Higuchi, T. (1983) The Visual and Spatial Structure of Landscapes. (Ed.) MIT Press, Cambridge, MA, (pp.1- 232).
54. Hillier, B. (1999). Space is the machine. Space Syntax, London, (pp. 1-355).
55. Hofierka, J., & Zlocha, M. (2012). A new 3-D solar radiation model for 3-D city models. *Transaction in GIS*, 16 (5):681-690.
56. Jakubowski, M., Guo, Q. & Kelly M. (2013). Tradeoffs between lidar pulse density and forest measurement accuracy. *Remote Sensing of Environment*, 130, 245–253.
57. Kamičaitytė-Virbašienė, J., Godienė, G. & Kavoliūnas, G. (2015). Methodology of visual pollution assessment for natural landscapes. *Journal of Sustainable Architecture and Civil Engineering*, (4)13, 80-88.
58. Kloucek, T., Lagner, O. & Símova, P. (2015) How does data accuracy influence the reliability of digital viewshed models? A case study with wind turbines. *Applied Geography*, 64, 46-54.
59. Koltsova, A., Tunçer, B. & Schmitt, G. (2013). Visibility Analysis for 3D Urban Environments. *eCAADe Computation and Performance*, Models of Computation: Human Factors 31 (2): 375-384.
60. Kułaga, Z., *et al*., (2011). Polish 2010 growth references for school-aged children and adolescents. *European Journal of Pediatrics*, 170 (5), 599–609.
61. Lake, M., W., Woodman, P. E. & Mithen, S. J. (1998). Tailoring GIS software for archeological applications: an example concerning viewshed analysis. *Journal of Archaeological Science* 25, 27-38.
62. Liang J., & Gong J. (2017). A Sparse Voxel Octree-Based Framework for Computing Solar Radiation Using 3D City Models. *ISPRS Int. J. Geo-Inf*., 6(4), 106: 1-15
63. Liu, X., Zhang, Z. and Peterson, J. & Chandra, S. (2007) The effect of LiDAR data density on DEM accuracy. *International Congress on Modelling and Simulation: Land, Water and Environmental Management: Integrated Systems for Sustainability*, 10-13 Dec., Christchurch, New Zealand.
64. Maloy, M., A. & Dean, D., J. (2001). An accuracy assessment of various gis-based viewshed delineation techniques. *Photogrammetric Engineering and Remote Sensing* 67(11), 1293-1298.
65. Marsh, J., E & Schreiber, K. (2015). Eyes of the empire: A viewshed-based exploration of Wari site-placement decisions in the Sondondo Valley, Peru. *Journal of Archaeological Science*, 4, 54–64.
66. Mitasova, H., Harmon, R. S., Weaver, K. J., Lyons, N. J., & Overton, M. F. (2012). Scientific visualization of landscapes and landforms. *Geomorphology*, 137(1), 122-137.
67. Morello, E., & Ratti, C. (2009). A digital image of the city: 3D isovists in Lynch's urban analysis. *Environment and Planning* B ,36(5), 837–853.
68. Murgoitio, J., Shrestha, R., Glenn, N. & Spaete, L. (2014). Airborne LiDAR and terrestrial laser scanning derived vegetation obstruction factor for visibility models. *Transactions in GIS*, 18 (1), 147–160.
69. Murgoitio, J., Shresthab, R., Glennb, F. & Spaeteb, L. (2013). Improved visibility calculations with tree trunk obstruction modelling from aerial LiDAR. *International Journal of Geographical Information Science*, 27(10), 1865-1883
70. Natapov, A. & Fisher-Gewirtzman, D. (2016). Visibility of urban activities and pedestrian routes: An experiment in a virtual environment. *Computers, Environment and Urban Systems*, 58, 60-70.
71. Natapov, A., Czamanski, D. & Fisher-Gewirtzman, D. (2013). Can visibility predict location? Visibility graph of food and drink facilities in the city. *Survey Review*, 45(333), 462–71.
72. Nourian, P., Gonçalves, R., Zlatanova, S., Arroyo Ohori, K., & Vu Vo, A. (2016). Voxelization algorithms for geospatial applications. MethodsX, 3, 69–86.
73. Nutsford, D., Reitsma, F., Pearson, A., L. & Kingham, S. (2015). Personalising the viewshed: visibility analysis from the human perspective. *Applied Geography*, 62, 1-7.
74. Oda, Y., Tsunekawa, K., & Hata, M., (2000). Advanced LOS path-loss model in microcellular mobile communications. *IEEE Transactions on Vehicular Technology*, 49(6), 2121-2125.
75. Ogburn, D., E. (2006). Assessing the level of visibility of cultural objects in past landscapes. *Journal of Archaeological Science*, 33, 405-413.
76. Olsen, R., Puetz, A. & Anderson, B. (2009). Effects of lidar point density on bare earth extraction and DEM creation. *ASPRS Annual Con.* Baltimore, Maryland, March 9-13.
77. Oregon Lidar Consortium (OLC), 2009. Minimum LiDAR data density consideration for Pacific Northwest Watershed Science, INC. http://www.oregongeology.org/sub/projects/olc/minimum-lidar-data-density.pdf (assessed: Sept. 2016).
78. O'Sullivan, D. & Turner, A. (2001). Visibility graphs and landscape visibility analysis. *International Journal of Geographical Information Science*, 15 (3), 221-237.
79. Peters, R., Ledoux, H. & Biljecki, F. (2015). Visibility analysis in a point cloud based on the medial axis transform. *Eurographics Workshop on Urban Data Modelling and Visualisation*, 23 November Delft, the Netherlands, (pp. 7–13).
80. Pirotti, F. & Tarolli, P. (2010). Suitability of LiDAR point density and derived landform curvature maps for channel network extraction. *Hydrological Processes*, 24(9): 1187–1197.

81. Portella, A., 2014. *Visual pollution: advertising, signage and environmental quality*. Farnharm: Ashgate Publishing, (p. 1-316).
82. Pyysalo, U., Oksanen, J. & Sarjakoski, T. (2009). Viewshed analysis and visualization of landscape voxel models, Satiago, *24th International Cartography Conference*, Chile, 15-21 November.
83. Raber G.T., Jensen J.R., Hodgson M.E., Tullis J.A., Davis B.A. & Berglund J. (2007). Impact of lidar nominal post-spacing on DEM accuracy and flood zone delineation. *Photogrammetric Engineering & Remote Sensing*. 73, 793–804.
84. Rasova, A. (2013). Fuzzy viewshed geoprocessing toolbox for ArcGIS: www.arcgis.com/home/item.html?id=5e9cb4fd73fe4288a4cf534cc5a119aa [accessed Sept 2016].
85. Ruiz, L., Hermosilla, T., Mauro, M. & Godino, M. (2014). Analysis of the influence of plot size and lidar density on forest structure attribute estimates, *Forests*, 5(5), 936-951.
86. Sahraoui, Y., Youssoufi, S. & Foltete J-H. (2016). A comparison of in situ and GIS landscape metrics for residential satisfaction modelling. *Applied Geography*, 74: 199-210
87. Schirpke, U., Tasser, E., & Tappeiner, U. (2013). Predicting scenic beauty of mountain regions. *Landscape and Urban Planning*, 111(1), 1–12.
88. Shaw, L. S. (1993). Geography: a place for GIS. *Applied Geography*, 13(2), 107-110.
89. Sindram, M., Machl, T., Steuer, H., Pültz, M., & Kolbe, T. H. (2016). Voluminator 2.0 -- speeding up the approximation of the volume of defective 3D building models. ISPRS Ann. Photogramm. Remote Sens. Spatial Inf. Sci., III-2, 29–36
90. Snyder, S., Whitmore, J., Schneider, I., & Becker, D. (2008). Ecological criteria, participant preferences and location models: A GIS approach toward ATV trail planning. *Applied Geography*, 28: 248-258.
91. Stoter, J. Ledoux, H. Reuvers, M. van den Brink, L., Klooster, R., Janssen, P., Beetz, J. Penninga, F., Vosselman, G. (2013). Establishing and implementing a national 3D standard in The Netherlands. *Photogramm.—Fernerkund.—Geoinf*, 2013: 381–392
92. Suleiman, W., Joliveau, T. & Favier, E. (2011). 3D urban visibility analysis with vector GIS data. Presented at the *GISRUK*, 26 April, University of Portsmouth, UK, (pp. 27-29).
93. Tan, L., M, Ficklin, L., D., Dixon, B., Ibrahim, L., A., Yusop, Z., & Chaplot, V. (2015). Impacts of DEM resolution, source, and resampling technique on SWAT-simulated streamflow. *Applied Geography*, 63: 357-368.
94. Tandy, C. R. V. (1967). The isovist method of landscape survey. In Murray H. C. (Ed.) *Methods of Landscape Analysis*, Landscape Research Group, London, (pp. 9–10).
95. Travis, M., R., Iverson, W., D., Gary, H., & Johnson, C. G. (1975). VIEWIT: computation of seen areas, slope, and aspect for land - use planning. Berkeley, California: USDA, Forestry Service, (p. 1-70).
96. Treitz, P., Lim, K., Woods, M., Pitt, D., Nesbitt, D. & Etheridge, D. (2012). LiDAR Sampling Density for Forest Resource Inventories in Ontario, Canada. *Remote Sensing, 4:* 830-848.
97. Turner, A., Doxa, M., O'Sullivan, D., & Penn, A. (2001). From isovists to visibility graphs: a methodology for the analysis of architectural space. *Environment and Planning B: Planning and Design*, 28(1), 103–121.
98. U.S. Geological Survey (USGS), National Geospatial Program, 2014. Base LiDAR specification version 1.2 by By Hans Karl Heidemann, (pp. 5)
99. Van den Berg, A., Van Lith, J., and Roos, J. (1985). Toepassing van het computer programma MAP2 in het landschapsbouwkundig onderzoek. *Landschap* 2(4); 278-293
100. Van Horn, J. E. & Mosurinjohn, N., A. (2010). Urban 3D GIS modeling of terrorism sniper hazards. *Social Science Computer Review*, 28(4), 482–496.
101. Wang, J., Robinson, G. J. and White, K., 1996. A fast solution to local viewshed computation using grid-based digital elevation models. Photogrammetric Engineering & Remote Sensing, 62, pp.1157– 64.
102. Wang, J., Robinson, G. J. and White, K. (2000). Generating viewsheds without using sightlines. *Photogrammetric Engineering & Remote Sensing*, 66: 87–90.
103. Wang, Y., Weinacker, H. & Koch, B. (2008). A Lidar Point Cloud Based Procedure for Vertical Canopy Structure Analysis And 3d Single Tree Modelling in Forest. *Sensors* 8(6): 3938–3951.
104. Wheatley, D. & Gillings, M. (2000). Vision, perception and GIS: developing enriched approaches to the study of archaeological visibility. In Lock G. (Ed.). *Beyond the Map: Archaeology and Spatial Technologies*, Amsterdam, IOS Press, (pp 1-27).
105. Weitkamp, G., Bregt, A., van Lammeren, R. & van den Berg, A. (2007). Three sampling methods for visibility measures of landscape perception. In: Winter, S. (Ed.), COSIT 2007, LNCS 4736. Springer-Verlag, Berlin, Heidelberg, (pp. 268–284).
106. Wrożyński, R., Sojka, M. & Pyszny, K. (2016). The application of GIS and 3D graphic software to visual impact assessment of wind turbines, *Renewable Energy*, (96) part A, 625- 635.
107. Wu, S., Li, J., & Huang G., H. (2008). A study on DEM-derived primary topographic attributes for hydrologic applications: Sensitivity to elevation data resolution. *Applied Geography*, 28: 210-223

108. Yang, P,. P, Putra, S., Y. & Li, W. (2007). Viewsphere: a GIS-based 3D visibility analysis for urban design evaluation. *Environment and Planning B: Planning and Design*, 34, 971 – 992.
109. Yang, B. (2016). GIS based 3-D landscape visualization for promoting citizen's awareness of coastal hazard scenarios in flood prone tourism towns. *Applied Geography*, 76: 85-97
110. Zhao, Y., Padmanabhan, A. & Wang, S. (2012). A parallel computing approach to viewshed analysis of large terrain data using graphics processing units. *International Journal of Geographical Information Science*, 27(2), 363–384.